

# Chemical abundances of the PRGs UGC7576 and UGC9796.

## I. Testing the formation scenario

M. Spavone<sup>1,2,\*</sup>, E. Iodice<sup>2</sup>, M. Arnaboldi<sup>3,4</sup>, G. Longo<sup>1,2</sup>, and O. Gerhard<sup>5</sup>

<sup>1</sup> Dipartimento di Scienze Fisiche, Università Federico II, via Cinthia 6, I-80126 Napoli, Italy

<sup>2</sup> INAF-Astronomical Observatory of Naples, via Moiarriello 16, I-80131 Napoli, Italy

<sup>3</sup> European Southern Observatory, Karl-Schwarzschild-Straße 2, D-85748 Garching bei München, Germany

<sup>4</sup> INAF, Osservatorio Astronomico di Pino Torinese, I-10025 Pino Torinese, Italy

<sup>5</sup> Max-Planck-Institut für Extraterrestrische Physik, Giessenbachstraße, D-85741 Garching bei München, Germany

Received February, 2011; accepted April, 2011

### ABSTRACT

**Context.** The study of the chemical abundances of HII regions in polar ring galaxies and their implications for the evolutionary scenario of these systems has been a step forward both in tracing the formation history of the galaxy and giving hints on the mechanisms at work during the building of disk by cold accretion process. It's now important to establish whether such results are typical for the class of polar disk galaxies as whole.

**Aims.** The present work aims at checking the cold accretion of gas through a “cosmic filament” as a possible scenario for the formation of the polar structures in UGC7576 and UGC9796. If these form by cold accretion, we expect the HII regions abundances and metallicities to be lower than those of same-luminosity spiral disks, with values of the order of  $Z \sim 1/10 Z_{\odot}$ , as predicted by cosmological simulations.

**Methods.** We have used deep long-slit spectra, obtained with DOLORES@TNG in the optical wavelengths, of the brightest HII regions associated with the polar structures to derive their chemical abundances and star formation rate. We used the *Empirical methods*, based on the intensities of easily observable lines, to derive the oxygen abundance  $12 + \log(O/H)$  of both galaxies. Such values are compared with those typical for different morphological galaxy types of comparable luminosity.

**Results.** The average metallicity values for UGC7576 and UGC9796 are  $Z = 0.4Z_{\odot}$  and  $Z = 0.1Z_{\odot}$  respectively. Both values are lower than those measured for ordinary spirals of similar luminosity and UGC7576 presents no metallicity gradient along the polar structure. These data, together with other observed features, available for the two PRGs in previous works, are compared with the predictions of simulations of tidal accretion, cold accretion and merging, to disentangle between these scenarios.

**Key words.** Galaxies: abundances – Galaxies: evolution – Galaxies: formation – Galaxies: individual: UGC7576, UGC9796 – Galaxies: peculiar – Methods: data analysis

## 1. Introduction

How galaxies acquire their gas is an open issue in the models of galaxy formation: recent theoretical works, supported by many numerical simulations, have argued that cold accretion plays a major role (Katz & White 1993; Katz et al. 1994; Kereš et al. 2005; Dekel & Birnboim 2006; Dekel & Birnboim 2008; Bournaud & Elmegreen 2009). Kereš et al. 2005 studied in detail the physics of the *cold mode* of gas accretion and they found that it is generally directed along filaments, allowing galaxies to draw gas from large distances. In particular, the cold accretion is a key mechanism to provide gas to disk galaxies (Brooks et al., 2009).

Recent simulations of disk formation in a cosmological context performed by Agertz et al. (2009) revealed that the so called chain-galaxies and clump-clusters, found only at higher redshifts (Elmegreen et al., 2007), are a natural outcome of early epoch enhanced gas accretion from cold dense streams as well as

tidally and ram-pressured stripped material from minor mergers and satellites. This freshly accreted cold gas settles into a large disk-like systems. This scenario reproduces the observed morphology and global rotation of disks, predicts a realistic metallicity gradient, and a star formation rate (SFR) of  $20M_{\odot}/yr$ . Agertz et al. (2009) found solar metallicity for the inner disk, while that in the clump forming region is only  $\sim 1/10Z_{\odot}$  due to the accretion of pristine gas in the cold streams mixed with stripped satellite gas.

Simulations also show that the interaction region between the new-formed disk and the cold streams can also result misaligned with the initial galactic disk: based on a very limited statistics, Agertz et al. (2009) suggest that this misalignment might not be typical, and it is due to a third cold stream that is perpendicular to the main filament. More recent analysis show that the accretion of gas along misaligned filaments with respect to the disk plane are more common and it leaves traces down to low redshift (Dekel et al. 2009; Roškar et al. 2010). An almost polar ring can result just as an extreme case of such process and,

\* e-mail: spavone@na.infn.it

as suggested by Agertz et al. (2009), it could be responsible for the formation of polar disks.

Hydrodynamical simulations performed by Macciò et al. (2006) and Brook et al. (2008) have shown that the formation of a polar disk galaxy can occur naturally in a hierarchical universe, where most low-mass galaxies are assembled through the accretion of cold gas infalling along a filamentary structures. According to Macciò et al. (2006), the polar disk forms from cold gas that flows along the extended  $\sim 1\text{Mpc}$  filament into the virialized dark matter halo. The gas streams into the center of the halo on an orbit that is offset from radial infall. As it reaches the center, it impacts with gas in the halo of the host galaxy and with the warm gas flowing along the opposite filament. Only the gas accreted perpendicular to the major axis of the potential can survive for more than a few dynamical lifetimes.

Brook et al. (2008) argued that polar disk galaxies are extreme examples of the misalignment of angular momentum that occurs during the hierarchical structure formation: an inner disk starts forming shortly after the last major merger at  $z \sim 2$ . Due to its gas rich nature, the galaxy rapidly forms a new disk whose angular momentum is determined by the merger orbital parameters. Later, gas continues to be accreted but in a plane that is almost perpendicular to the inner disk. At  $z \sim 0.8$  the central galaxy is still forming stars in a disk, while the bulk of new star formation is in a highly inclined polar disk. By  $z \sim 0.5$  the inner disk has exhausted its gas, while gas continues to fall onto the polar disk. From this point on, star formation occurs exclusively in the polar disk, that remains stable for at least 3 Gyrs. The formation mechanisms described above can self-consistently explain both morphology and kinematics of a polar disk galaxy. In particular, the predictions turn out to be consistent with many features (like colors and color gradients, longevity, spiral arms, HI content and distribution) observed for the polar disk galaxy NGC4650A.

NGC4650A is the prototype of the wide Polar Ring Galaxies (PRGs) and has been studied in detail to understand its formation and physical properties (Arnaboldi et al. 1997; Gallagher et al. 2002; Iodice et al. 2002; Swaters & Rubin 2003; Bournaud & Combes 2003; Iodice et al. 2006) in order to constrain many of the processes at work during galaxy interactions and merging. Very recently, Spavone et al. (2010), by using deep longslit spectroscopy with FORS2@ESO-VLT, studied the abundance ratios and metallicities of the HII regions associated to the polar disk in NGC4650A, in order to test the cold accretion scenario for this object. The chemical abundance is one of the key parameters that can be estimated in a galaxy disk and directly compared with the theoretical predictions: in fact, if the gas is essentially primordial it should have a very low abundance of heavy elements.

Main results obtained for NGC4650A show i) that it has metallicity lower than spiral galaxy disks of the same total luminosity, where  $Z = 0.2Z_{\odot}$ , which is consistent with values predicted for the formation of disks by cold accretion processes (Agertz et al., 2009); ii) the absence of any metallicity gradient along the polar disk, which suggests that the metal enrichment is not influenced by the stellar evolution of the older central spheroid and, thus, the disk was formed later by the infall of metal-poor gas from outside which is still forming the disk. The latter is also a characteristic found in some other PRGs (Brosch et al., 2009) and in LSB galaxies (de Blok & van der Hulst, 1998), that have colors, metallicities, age and brightness similar to those of PRGs suggesting that the infall of metal-poor gas may reasonably fit all these observational evidences. Spavone et al. (2010) lead the way to imple-

ment a test for the cold accretion. Such study has revealed an indirect and well-based check for the cold accretion scenario of disk formation. In this work we would like to perform the same kind of analysis on the two PRGs UGC7576 and UGC9796. These two objects are similar to NGC4650A; such a morphological similarity may suggest a similar formation mechanism: the polar structures are more extended with respect to the central spheroids, thus, as NGC4650A, they were classified as wide PRG (Whitmore et al., 1990); they are characterized by exponential surface brightness profiles, very blue colors, knotty appearance and large amount of HI gas all associated to these components. The most relevant feature in UGC9796 is that the HI distribution resemble that of a disk in differential rotation, rather than a ring (Reshetnikov et al. 1994; Cox et al. 2006), like in NGC4650A (Arnaboldi et al., 1997). Given the new results obtained for NGC4650A it is now important to establish whether the lack of metallicity gradient and low metallicity, and the inferred accretion of low-metallicity material after the formation of the central spheroid, are typical for the class of wide PRGs as a whole: to this aim we have studied the PRGs UGC7576 and UGC9796, that are suitable systems to investigate this question further.

### 1.1. UGC7576

UGC7576 (Fig. 1) is a kinematically confirmed Polar Ring Galaxy (Whitmore et al., 1990) and its main properties are listed in Tab. 1. This object is at a distance of about 94 Mpc, based on  $H_0 = 75\text{ km s}^{-1}\text{ Mpc}^{-1}$  and heliocentric radial velocity of  $V = 7022\text{ km s}^{-1}$ , which implies that  $1\text{ arcsec} = 0.45\text{ kpc}$ . The kinematics shows that the polar structure of UGC7576 is more similar to a ring rather than a disk, given that the rotation curve does not show differential rotation, contrary to those of NGC4650A and UGC9796. Reshetnikov et al. (1994) studied the global morphology of UGC7576 and they were able to distinguish three components: *i*) the main central body with elliptical isophotes, *ii*) a narrow polar ring crossing the central region of the main galaxy, *iii*) a faint outer envelope. The gradient of the surface brightness distribution of the central galaxy decrease at  $r \geq 20''$ , while both B-V and V-R color indices slightly decrease with radius.

The distribution of color indices is slightly asymmetric, suggesting that the polar ring is projected not exactly on the nucleus but with a small NW displacement. The color asymmetry correlates with the asymmetry in the hydrogen distribution (Schechter et al., 1984). Moreover, the plane of the disk reveals a warping, which suggests that the ring has not settled yet in the equilibrium plane.

Surface brightness distribution along the major axis of the ring is very symmetric and the surface brightness is approximately constant ( $\mu_B \sim 24.3$ ) up to  $r \sim 35''$ , then falls abruptly. Also the colors have no evident changes within the region of constant brightness.

UGC7576 is also embedded in a faint outer envelope, whose major axis position angle coincides with the position angle of the polar ring and this suggests a common origin for both components (Reshetnikov et al., 1994).

Reshetnikov & Combes (1994) have analyzed the  $H_{\alpha}$  spectroscopy for a sample of PRGs, including both UGC7576 and UGC9796. In the case of UGC7576, the  $H_{\alpha}$  rotation curve along the polar structure was consistent with the HI rotation curve obtained by Schechter et al. (1984) and both curves are straight lines with the same gradient: this let the authors to conclude that the ring is, more reliable, an edge-on narrow annulus. By assum-

ing a spherical mass distribution, Reshetnikov & Combes (1994) estimated a total mass-to-light ratio of  $M/L_B \sim 11.3M_\odot/L_\odot$  within the last measured point of the rotation curve (where the velocity reaches its maximum value): this value, together with the  $M/L_B$  for UGC9796, is among the highest  $M/L_B$  estimated for the whole sample of PRGs. Reshetnikov & Combes (1994) also performed a simple dynamical mass model for both PRGs studied in this work: in the hypothesis of a spherical dark halo, for UGC7576 they found a dark-to-luminous mass ratio of about 1.3, inside the polar ring radius.

## 1.2. UGC9796

UGC9796 (Fig. 2), also known as IIZw 73, is at a distance of about 72 Mpc based on  $H_0 = 75 \text{ km s}^{-1} \text{ Mpc}^{-1}$  and heliocentric radial velocity of  $V = 5406 \text{ km s}^{-1}$ , which implies that 1 arcsec = 0.35 kpc. It has one of the most non-polar PRG. Its apparent major axis in fact is only  $65^\circ$  from the major axis of the central S0 rotationally supported galaxy and this implies a rapid rate of differential precession. The polar structure is less symmetric than in UGC7576 and the distribution of the colors is also asymmetric, with the NE side considerably redder than the SW side. The color asymmetry coincides with the asymmetry of the HI density distribution. The HI gas is all associated with the polar structure, which thus contains as many baryons as the host galaxy (Schechter et al., 1984), and shows a central hole at about  $25''$ . The huge mass-to-light ratio of  $M_{\text{dyn}}/L_B \simeq 50$  in solar units, lead Cox et al. (2006) to conclude that most of the mass in this system is dark. As in the case of UGC7576, the  $H_\alpha$  rotation curve (Reshetnikov & Combes, 1994) is in good agreement with the HI rotation curve (Schechter et al., 1984). The shape of the rotation curve indicates that this component is actually a differentially rotating disk, rather than a ring, very similar to the polar disk in NGC4650A.

In Tab. 1 we summarize the photometric and HI observed quantities for UGC7576 and UGC9796 and we add those of NGC4650A for reference in the same table.

## 2. Observation and data reduction

The spectra analyzed in this work were obtained with DOLORES@TNG (Device Optimized for the LOW RESolution), in visitor mode during the observing run A21TAC-54 (on May 2010). DOLORES is installed at the Nasmyth B focus of the TNG and is equipped with the E2V 4240 CCD with an angular resolution of  $0''.252 \text{ pix}^{-1}$ . The adopted slit was  $2''$  wide and it was aligned along both the North and South side of the polar structures of the two galaxies UGC7576 and UGC9796, at  $P.A. = 53^\circ$  and  $P.A. = 16^\circ$  respectively (see Fig. 3), in order to include the most luminous HII regions in the polar structures. The total integration time for each object is 4 hrs, with an average seeing of  $1''.2$ .

At the systemic velocities of UGC7576 and UGC9796, to cover the red-shifted emission lines of  $[OII]\lambda 3727$ ,  $H_\gamma(\lambda 4340)$ ,  $[OIII]\lambda 4363$ ,  $[OIII]\lambda 4959$ ,  $5007$ ,  $H_\beta(\lambda 4861)$  and  $H_\alpha(\lambda 6563)$ , the grism LR-B was used in the 3600–6800Å wavelength range, with a dispersion of  $2.52 \text{ \AA/pix}$ .

The data reduction was carried out using the CCDRED package in the IRAF<sup>1</sup> (*Image Reduction and Analysis Facility*) envi-

ronment. The main strategy adopted for each data-set included dark subtraction<sup>2</sup>, flat-fielding correction, sky subtraction and rejection of bad pixels. Wavelength calibration was achieved by means of comparison spectra of Hg+Ne lamps acquired for each observing night, using the IRAF TWODSPECLONGSLIT package. The sky spectrum was extracted at the outer edges of the slit, for  $r \geq 30 \text{ arcsec}$  from the galaxy center, where the surface brightness is fainter than  $24 \text{ mag/arcsec}^2$ , and subtracted off each row of the two dimensional spectra by using the IRAF task BACKGROUND in the TWODSPECLONGSLIT package. On average, a sky subtraction better than 1% was achieved. The sky-subtracted frames were co-added to a final median averaged 2D spectrum.

The final step of the data-processing is the flux calibration of each 2D spectra, by using observations of the standard star Feige66 and the standard tasks in IRAF (STANDARD, SENSFUNC and CALIBRATE). To perform the flux calibration we extracted a 1-D spectrum of the standard star to find the calibration function; then we extracted a set of 1-D spectra of the galaxy summing up a number of lines corresponding to the slit width. Since the slit width was  $2''$  and the scale of the instrument was  $0.252''/\text{pix}$ , we collapsed eight lines to obtain each 1-D spectrum. Finally we applied the flux calibration to this collection of spectra. The wavelength and flux-calibrated spectra are shown in Fig. 4 and Fig. 5.

The fluxes of the above mentioned emission lines were measured using the IRAF SPLOT routine, that provides an interactive facility to display and analyze spectra. We evaluated flux and equivalent width by marking two continuum points around the line to be measured. The linear continuum is subtracted and the flux is determined by simply integrating the line intensity over the local fitted continuum. The errors on these quantities are calculated, following Pérez-Montero & Díaz (2003), by the relation  $\sigma_1 = \sigma_c N^{1/2} [1 + EW/(N\Delta)]^{1/2}$ , where  $\sigma_1$  is the error in the line flux,  $\sigma_c$  is the standard deviation in a box near the measured line and represents the error in the continuum definition, N is the number of pixels used to measure the flux, EW is the equivalent width of the line and  $\Delta$  is the wavelength dispersion in  $\text{Å/pixel}$ .

### 2.1. Reddening correction

Reduced and flux calibrated spectra and the measured emission line intensities were corrected for the reddening, which account both for that intrinsic to the source and to the Milky Way. By comparing the intrinsic Balmer decrement  $H_\alpha/H_\beta = 2.89$ , we derived the visual extinction  $A(V)$  and the color excess  $E(B-V)$ , by adopting the mean extinction curve by Cardelli et al. (1989)  $A(\lambda)/A(V) = a(x) + b(x)R_V$ , where  $R_V[\equiv A(V)/E(B-V)] = 3.1$  and  $x = 1/\lambda$ . All the emission lines in our spectra are in the *optical/NIR* range (see Cardelli et al. 1989), so we used the average  $R_V$ -dependent extinction law derived for these intervals to perform the reddening correction.

We derived the average observed Balmer decrements for both galaxies, which are the following:

$$(H_\alpha/H_\beta)_{\text{UGC7576}} = 3.18 \pm 2.10$$

$$(H_\alpha/H_\beta)_{\text{UGC9796}} = 2.24 \pm 1.30$$

while the color excess obtained by using these observed decrements are:

$$[E(B-V)]_{\text{UGC7576}} = 0.09 \pm 0.36$$

$$[E(B-V)]_{\text{UGC9796}} = -0.25 \pm 0.92.$$

The negative value of the color excess for UGC9796 indicates

<sup>1</sup> IRAF is distributed by the National Optical Astronomy Observatories, which is operated by the Associated Universities for Research in Astronomy, Inc. under cooperative agreement with the National Science Foundation.

<sup>2</sup> Bias frame is included in the Dark frame.

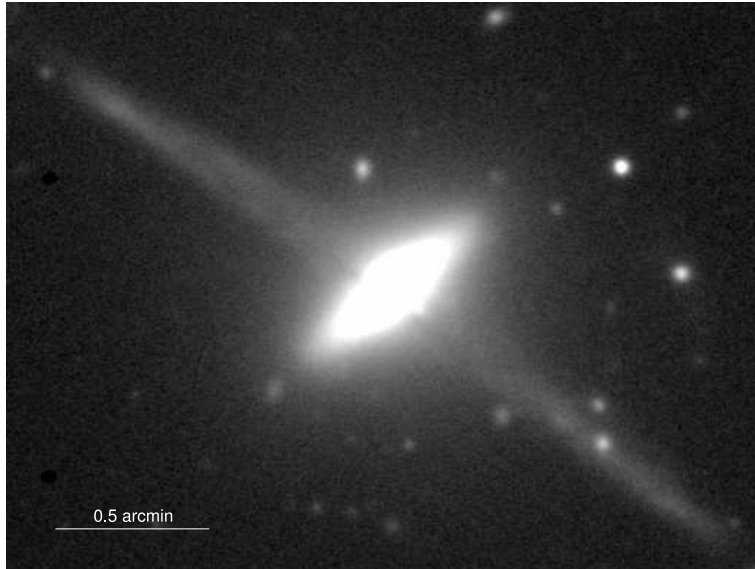


**Fig. 1.** R-band image of the Polar Ring Galaxy UGC7576

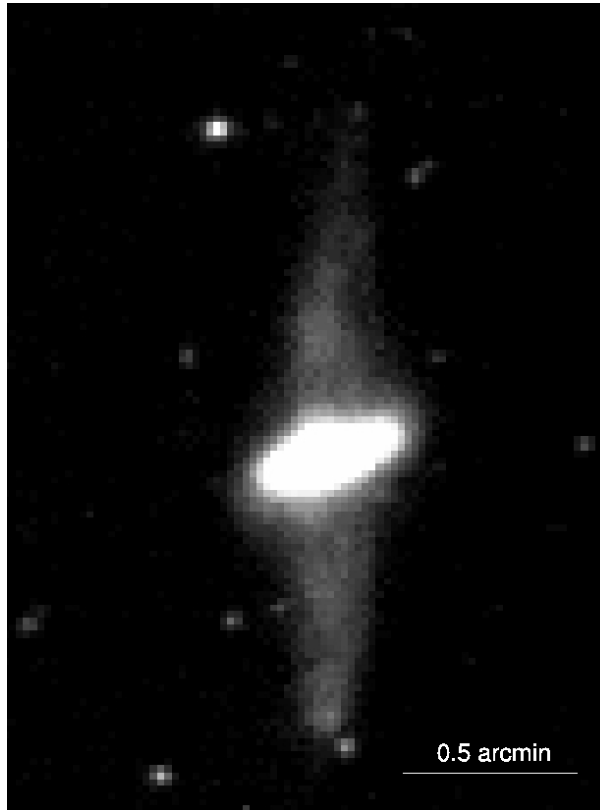


**Fig. 2.** Optical image of the Polar Ring Galaxy UGC9796, obtained by the authors at TNG telescope.

the presence of stars that are bluer and hotter than normal, and thus they have V apparent magnitude greater than the B one, leading to a negative B-V color. In general, stars hotter than Vega, that have  $E(B - V) = 0$ , have negative color excess (Masana et al., 1998).

Such values of  $E(B-V)$  are used to derive the extinction  $A_\lambda$ , through the Cardelli's law. Finally, the corrected fluxes are given by

$$\frac{F_{int}^\lambda}{F_{int}^{H\beta}} = \frac{F_{obs}^\lambda}{F_{obs}^{H\beta}} 10^{0.4[A_\lambda - A_{H\beta}]} \quad (1)$$

### 3. Empirical oxygen abundances determination

The analysis of nebular spectra in HII regions is the best tool for the determination of chemical abundances in spiral and irregular galaxies. The abundances of several elements can be determined by using strong emission lines clearly visible in the spectra.

The main aim of this work is to measure the *Oxygen abundance parameter*  $R_{23} = ([OII]\lambda 3727 + [OIII]\lambda\lambda 4959 + 5007)/H\beta$  (Pagel et al., 1979), and consequently the oxygen abundance  $12 + \log(O/H)$  and the metallicity of the HII regions in the po-

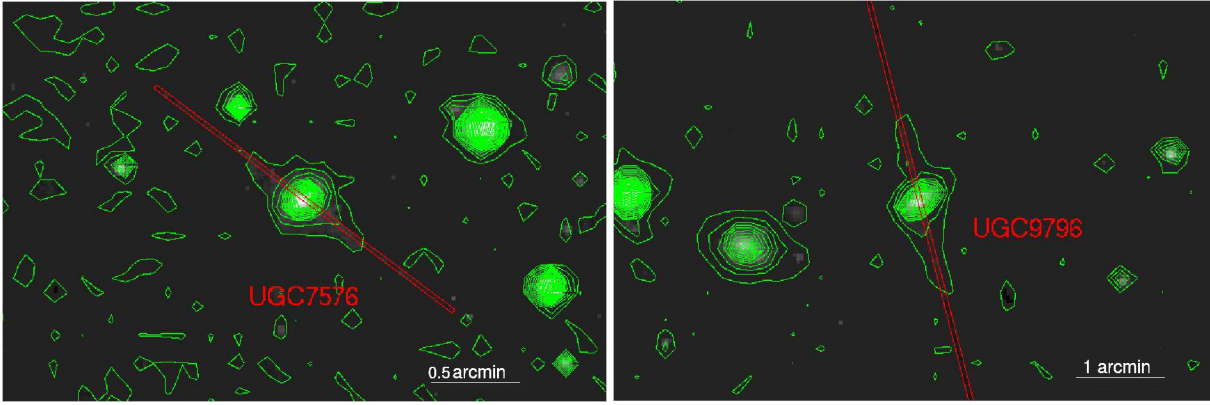


**Fig. 3.** Optical image of UGC7576 (left) and UGC9796 (right), with superimposed slits used to acquire data analyzed in this work.

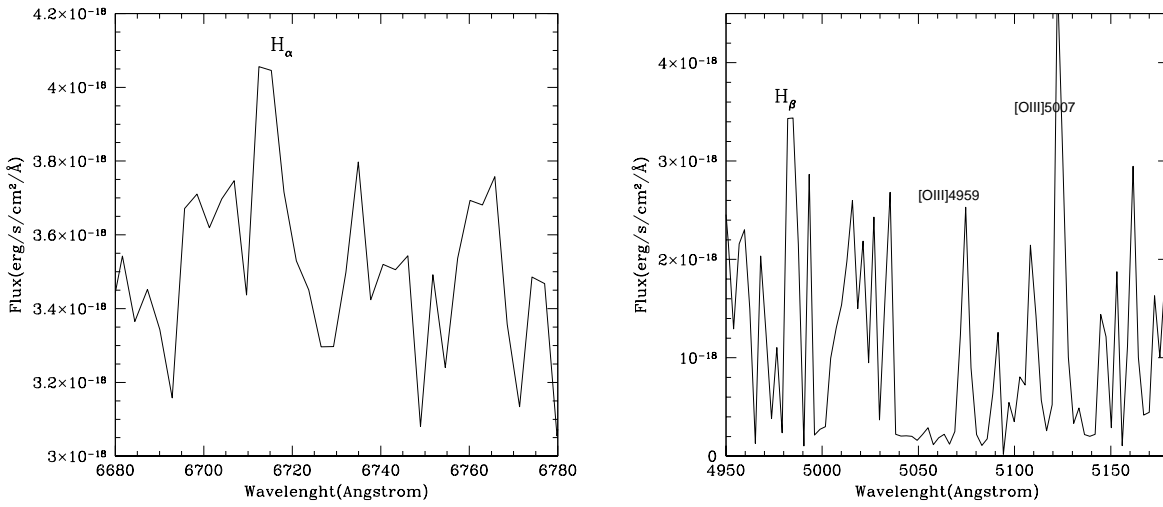


**Fig. 4.** Spectrum of UGC7576 obtained by summing up 1D spectra extracted along both the North and South side of the polar structure.

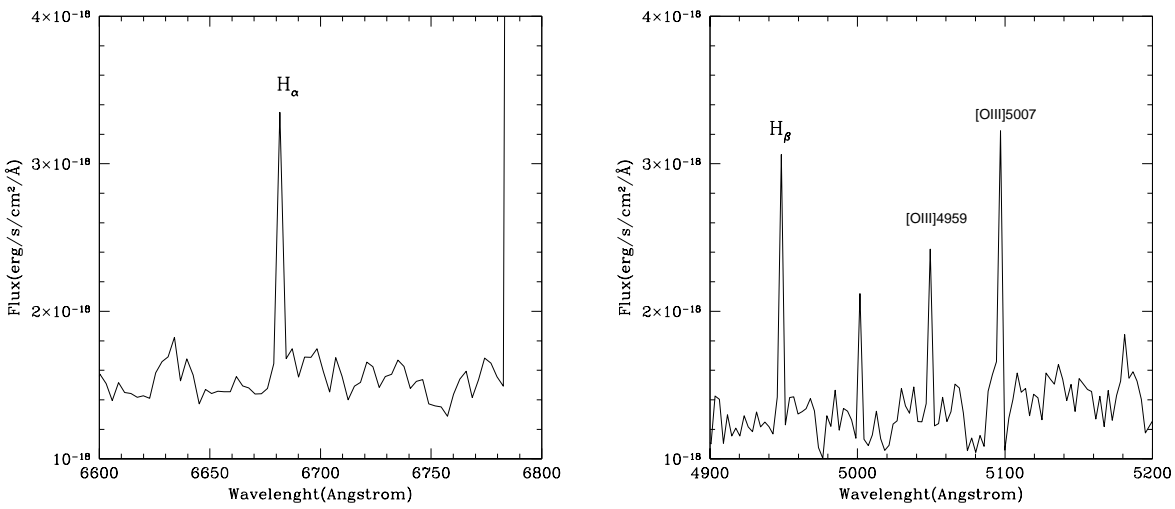


**Fig. 5.** Spectrum of UGC9796 obtained by summing up 1D spectra extracted along both the North and South side of the polar structure.

lar disks of UGC7576 and UGC9796, following the procedure outlined by Spavone et al. (2010) for NGC4650A.

The *Empirical methods* are based on the cooling properties of ionized nebulae which translate into a relation between emission-line intensities and oxygen abundance. Several abundance calibrators have been proposed based on different emission-line ratios:  $R_{23}$  (Pagel et al., 1979),  $S_{23}$  (Díaz & Pérez-Montero, 2000); among the other, in this work we used the so called P-method introduced by Pilyugin (2001).

Pilyugin (2001) realized that for fixed oxygen abundances the value of  $X_{23} = \log R_{23}$  varies with the excitation parameter  $P = R_3/R_{23}$ , where  $R_3 = OIII[4959 + 5007]/H\beta$ , and proposed that this latter parameter could be used in the oxygen abundance determination. This method, called ‘‘P-method’’, propose to use a more general relation of the type  $O/H = f(P, R_{23})$ , compared with the relation  $O/H = f(R_{23})$  used in the  $R_{23}$  method. The equation related to this method is the following

$$12 + \log(O/H)_P = \frac{R_{23} + 54.2 + 59.45P + 7.31P^2}{6.07 + 6.71P + 0.371P^2 + 0.243R_{23}} \quad (2)$$

where  $P = R_3/R_{23}$ . It can be used for oxygen abundance determination in moderately high-metallicity HII regions with undetectable or weak temperature-sensitive line ratios Pilyugin (2001). The definition of moderately high metallicity is adopted from Pilyugin (2001) and refers to the abundance interval  $8 < 12 + \log O/H < 8.5$  where the relation  $O/H = F(R_{23})$  (Pagel et al., 1979) becomes degenerate. As suggested by Pilyugin (2001), the positions of HII regions in the  $P - R_3$  diagram are related to their oxygen abundances. Since both PRGs are in the region where moderately high-metallicity HII regions are located, we can use Eq. 2 above to estimate the oxygen abundances for both UGC7576 and UGC9796.

We estimate the mean oxygen abundance parameter,  $R_{23}$ , by summing the fluxes of the nebular emission lines at different regions along the polar structures (see Tab. 2). The average values of oxygen abundance obtained for UGC7576 and UGC9796 are  $12 + \log(O/H)_P = 8.5 \pm 0.5$  and  $12 + \log(O/H)_P = 7.7 \pm 1$  respectively (see Tab. 3). Moreover, for UGC7576 it has been possible to measure the oxygen abundance  $12 + \log(O/H)_P$  at different distances from the center of the galaxy and the values are shown in Fig. 7.

## 4. Metallicity and SFR estimates

We derive the oxygen abundance  $12 + \log(O/H)$  for UGC7576 and UGC9796, by using the empirical P-method (Pilyugin, 2001). We found  $12 + \log(O/H) = 8.5 \pm 0.5$  for UGC7576 and  $12 + \log(O/H) = 7.7 \pm 1$  for UGC9796. The metallicities corresponding to each value of oxygen abundances given before have been estimated. We adopted  $12 + \log(O/H)_\odot = 8.83 \pm 0.20 = A_\odot$  and  $Z_\odot = 0.02$  (Asplund et al., 2004). Given that  $Z \approx KZ_\odot$ ,  $K_{UGC7576} = 10^{[A_{UGC7576} - A_\odot]}$  and  $K_{UGC9796} = 10^{[A_{UGC9796} - A_\odot]}$ , we obtain metallicities for the HII regions of the polar disk of  $Z \approx 0.008$  in UGC7576 and  $Z \approx 0.002$  in UGC9796 which correspond respectively to  $Z \approx (0.400 \pm 0.002)Z_\odot$  and  $Z \approx (0.100 \pm 0.001)Z_\odot$ , in good agreement with the values obtained by Radtke et al. (2003) (see Tab. 3).

### 4.1. Metallicity-luminosity relation

The mean values for the oxygen abundance along the polar structure of UGC7576 and UGC9796, derived by the empirical method (see sec. 3), are compared with those for a sample of late-type disk galaxies by Kobulnicky & Zaritsky (1999),

as function of the total luminosity. To this aim, we converted the absolute blue magnitude for the objects in the sample of Kobulnicky & Zaritsky (1999) by using  $H_0 = 75$  km/s/Mpc. Results are shown in Fig. 6.

We found that UGC7576 is located in the region where spiral galaxies are found, and, contrary to its high luminosity, it has metallicity lower than spiral galaxy disks of the same total luminosity and it is consistent with that observed for NGC4650A.

UGC9796 instead is even more metal-poor than UGC7576 and NGC4650A, in fact it is located in the region where HII and irregular galaxies are also found, characterized by lower luminosities and metallicities with respect to the spiral galaxies.

We also compare our new results with those obtained by Perez-Montero et al. (2009) for IIZw71, a blue compact dwarf galaxy also catalogued as a probable polar ring: consistently with its low luminosity, the metallicity of the brightest knots in the ring of IIZw71 is lower with respect to that of UGC7576, but it is slightly higher than those of UGC9796. Taking into account the total magnitude, such values are somewhat lower than that expected by the metallicity-luminosity relation.

### 4.2. Star formation rate

The  $H_\alpha$  emission is detected in both systems with adequate signal-to-noise, and from the measured integrated flux we can derive the star formation rate in the polar ring structure. We have derived the SFR for the polar structures of UGC7576 and UGC9796, from the  $H_\alpha$  luminosity using the expression given by Kennicutt (1998)  $SFR = 7.9 \times 10^{-42} \times L(H_\alpha)$ . We find that it is almost constant along the disks of both galaxies, within a large scatter in the individual values. From the average values of  $L(H_\alpha) \approx 2.36 \times 10^{36}$  erg/s for UGC7576 and  $L(H_\alpha) \approx 5.33 \times 10^{35}$  erg/s for UGC9796, we have obtained an average  $SFR \sim 1.9 \times 10^{-5} M_\odot/\text{yr}$  and  $SFR \sim 4.2 \times 10^{-6} M_\odot/\text{yr}$  respectively. These values are significantly lower than those obtained for NGC4650A (Spavone et al., 2010), which is  $SFR \sim 0.06 M_\odot/\text{yr}$  and IIZw71 (Perez-Montero et al., 2009), which is  $SFR \sim 0.035 M_\odot/\text{yr}$ .

Taking into account that the polar structure in both PRGs is very young, since the last burst of star formation occurred less than 1 Gyr ago (Reshetnikov & Combes, 1994), we check if the present SFR and even 2 and 3 times higher (i.e.  $SFR = 3.8 \times 10^{-5} M_\odot/\text{yr}$ ,  $SFR = 5.7 \times 10^{-5} M_\odot/\text{yr}$  and  $SFR = 8.4 \times 10^{-6} M_\odot/\text{yr}$ ,  $SFR = 1.26 \times 10^{-5} M_\odot/\text{yr}$ ), can give the inferred metallicities of  $Z = 0.4Z_\odot$  (for UGC7576) and  $Z = 0.1Z_\odot$  (for UGC9796) and how strongly could increase the metallicity with time.

Given the presence of star forming regions in the polar disk of NGC4650A, Spavone et al. (2010) used a constant SFR law for this object. In the case of UGC7576 and UGC9796, the redder B-V color and the lower  $M_{HI}/L_B$  suggest a longer time since the last burst of star formation in these objects. Furthermore the difference in the detected  $H_\alpha$  fluxes and consequently of the SFR of these galaxies are consistent with it (see Tab. 1). Given these observational properties and the absence of star forming clumps, we adopted an exponentially declining SFR started several Gyrs ago: this is typically used for late-type galaxies because, on average, it gives even older stars than a linear decay. The expression is:  $SFR(t) = M_\star \tau^{-1} \exp[-(t_0 - t)/\tau]$ , where we assume  $t_0 = 8 \text{ Gyrs}$ , because in  $\Lambda$ CDM models such cold accretion is more unlikely at low redshifts,  $\tau = 2 \text{ Gyrs}$  is the decay timescale and  $t$  is the lookback time (Bruzual & Charlot, 2003).

By using the mass-metallicity relation derived by Tremonti et al. (2004), where  $12 + \log(O/H) = -1.492 + 1.847 \log(M_\star) - 0.08026(\log M_\star)^2$ , we found

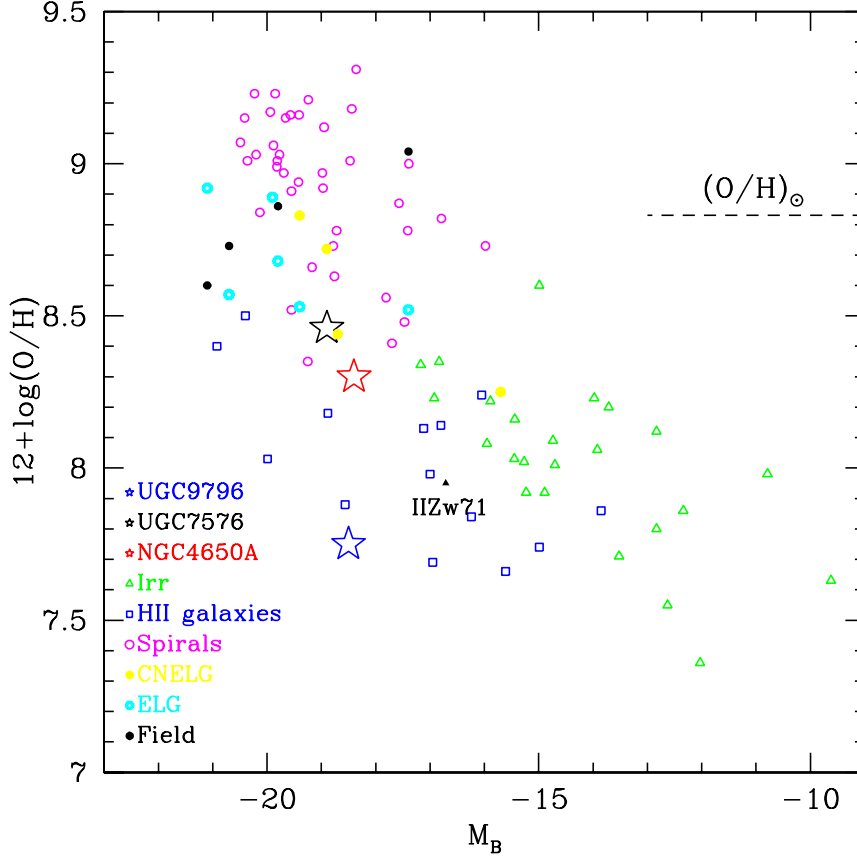


**Fig. 6.** Oxygen abundance vs absolute blue magnitude for Compact Narrow Emission-Line Galaxies (CNELGs, yellow filled circles), star-forming Emission Line Galaxies (ELGs, cyan open circles), four field galaxies with emission lines (filled black circles), nearby dwarf irregulars (open triangles), local spiral galaxies (open circles), local HII galaxies (open squares), NGC4650A (red star) (Spavone et al. 2010), the polar disk galaxy IIZw71 (Perez-Montero et al.2009), UGC7576 (black star) and UGC9796 (blue star) (this work). The dashed line indicates the solar oxygen abundance.

that for UGC7576  $0.5Z_{\odot} \leq Z \leq 1Z_{\odot}$  and for UGC9796  $0.05Z_{\odot} \leq Z \leq 0.45Z_{\odot}$ . This shows that the present SFR for the polar structures is able to increase the metallicity of about  $0.15 Z_{\odot}$  for UGC7576 and  $0.05 Z_{\odot}$  for UGC9796, after 1Gyr. We also derived the expected metallicities by using different values for the free parameters  $\tau$  (the decay timescale) and  $t_0$ , in order to check how these parameters can change the metallicity range: we found that the obtained metallicities are comparable, or even lower, than those reported above, with differences of about 4%.

For UGC7576 the derived values for  $Z$  are larger than  $Z = 0.400 \pm 0.002Z_{\odot}$  found by using the element abundances (see Sec.3); for UGC9796, instead, we found that the metallicity of  $Z = 0.100 \pm 0.001Z_{\odot}$ , estimated by using the element abundances, falls near the lower limit of the range of expected metallicities. The implications of these results will be discussed in details in Sec. 5.

#### 4.3. Metallicity gradient along the polar structure of UGC7576

The oxygen abundance in the polar ring of UGC7576 as a function of the radius derived by empirical methods is shown in Fig. 7: the plot shows that the metallicity remains almost constant along the projected major axis of the polar ring. It is only slightly declining, differently from what it is observed for spiral galax-

ies, where there is a very steep gradient in metallicity. The absence of metallicity gradient is a typical behavior found in LSB galaxies (de Blok & van der Hulst, 1998), and also in the polar disk galaxy studied by Brooks et al. (2009) and in NGC4650A (Spavone et al., 2010). This suggests that, as already pointed out for NGC4650A (Spavone et al., 2010), the star formation and the metal enrichment in the polar structure is not influenced by the stellar evolution of the central spheroid and that the polar ring was formed later. As also suggested by Rupke et al. (2010), numerical simulations predict that the absence of metallicity gradient is accounted for by inflow of low metallicity gas from the outskirts.

On the contrary, ordinary and oxygen-rich spiral galaxies, where no primordial gas is accreted from outside, show a decreasing abundance with increasing radii (see Fig. 7 and Pilyugin et al. 2006). These observed features in spiral disks are well explained by the infall models of galaxy formation: they predict that these systems build up through the accretion of on-site gas, which become more metal rich while it flows towards the galaxy center (Matteucci & Francois 1989; Boissier & Prantzos 1999). Such process generates the observed gradients.

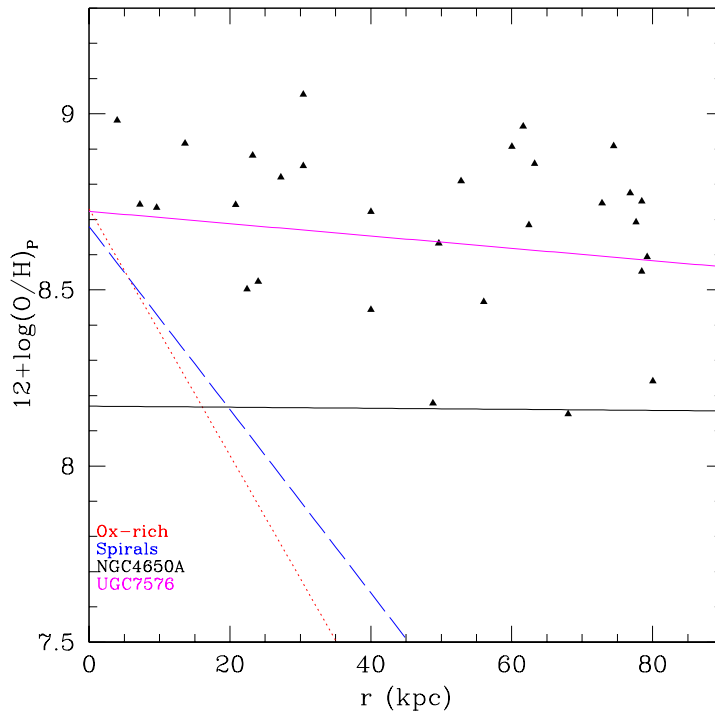


**Fig. 7.** Oxygen abundance of UGC7576 derived with P- method, proposed by Pilyugin (2001), versus radius. The superimposed lines are the linear best fit derived by Pilyugin et al. (2006); the red line represents the best fit to the abundance of oxygen-rich spirals, while the blue line is those related to ordinary spirals. The black line is the best fit obtained for NGC4650A, while the magenta line is the best fit obtained for UGC7576.

## 5. Formation history for UGC7576 and UGC9796: discussion and conclusions

Galaxies with a polar ring/disk have a special role in the studies of physical processes at work during galaxy interactions and merging. In order to account both for the featureless morphology of the central spheroidal galaxy and for the more complex structure of the polar ring/disk, so far three main formation processes have been proposed: *i*) a major dissipative merger; *ii*) tidal accretion of material (gas and/or stars) by outside; *iii*) cold accretion of pristine gas along a filament.

In the merging scenario, the PRG results from a “polar” merger of two disk galaxies with unequal mass, (Bekki 1997; Bekki 1998; Bournaud et al. 2005). In the accretion scenario, the polar ring/disk may form by a) the disruption of a dwarf companion galaxy orbitating around an early-type system, or by b) the tidal accretion of gas stripping from a disk galaxy outskirts, captured by an early-type galaxy on a parabolic encounter (Reshetnikov & Sotnikova 1997; Bournaud & Combes 2003; Hancock et al. 2009). Both major merger and accretion scenarios are able to account for many observed PRGs morphologies and kinematics, such as the existence of both wide and narrow rings, helical rings and double rings (Whitmore et al., 1990).

The cold accretion scenario has been proposed very recently for the formation of a wide disk-like polar rings (see Sec. 1): a long-lived polar structure may form through cold gas accretion along a filament, extended for  $\sim 1$  Mpc, into the virialized dark matter halo (Macciò et al., 2006). In this formation scenario, there is no limits to the mass of the accreted material, thus a very massive polar disk may develop either around a stellar disk or a spheroid.

As suggested by the previous studies on PRGs (Spavone et al. 2010, Iodice et al. 2006), the critical physical parameters that allow to discriminate among the three formation scenarios are 1) the total baryonic mass (stars plus gas) observed in the polar structure with respect to that in the central spheroid; 2) the kinematics along both the equatorial and meridional planes; 3) the metallicity and SFR in the polar structure.

In the tidal accretion scenario the total amount of accreted gas by the early-type object is about 10% of the gas in the disk donor galaxy, i.e. up to  $10^9 M_{\odot}$ . In the case of UGC7576 and UGC9796, the polar structure is characterized by a high baryonic mass (see Tab. 4), comparable with the total luminous mass in the central spheroid. Similarly to the case of NGC4650A (Spavone et al., 2010), the large HI mass exclude the formation of the polar structures through the tidal accretion of gas and stars by an external donor galaxy (Bournaud & Combes, 2003).

In the merging scenario, the morphology and kinematics of the merger remnants depends on the merging initial orbital parameters and the initial mass ratio of the two galaxies (Bournaud et al., 2005). In the case of UGC7576 and UGC9796, this scenario is ruled out because, according to simulations (e.g. Bournaud et al. 2005), a high mass ratio of the two merging galaxies is required to form a massive and extended polar disk as observed in both the PRGs: this would convert the intruder into an elliptical-like, not rotationally supported, stellar system. Since this is in contrast with the high maximum rotation velocities observed (see Reshetnikov & Combes 1994 and Tab. 4) in UGC7576 ( $\sim 212 \text{ km/s}$ ) and UGC9796 ( $\sim 157 \text{ km/s}$ ), the merging scenario is ruled out for both galaxies.

As already mentioned, if the polar structure, both around an elliptical and disk galaxy, forms by the cold accretion of gas

from filaments there is no limit to the accreted mass. Moreover, due to the inflow of pristine gas, the metallicity is lower with respect to that observed in galaxies of comparable total luminosity, and its value derived by the present SFR is higher than those directly measured by the chemical abundances. Spavone et al. (2010) have found that such predictions were consistent with observations in the polar disk galaxy NGC4650A, yielding to the conclusion that the cold accretion of gas by cosmic web filaments is the most realistic formation scenario for this object.

By studying the chemical abundances in the polar structure of UGC7576 and UGC9796, in the present work we aim at testing the cold accretion scenario for these objects. The main results are as follows (see also Sec. 4): 1) both PRGs have on average lower metallicity with respect to that of same-luminosity spiral disks, in particular, for UGC7576  $Z = 0.4Z_{\odot}$  and for UGC9796  $Z = 0.1Z_{\odot}$ ; 2) the metallicity expected for the present SFR at three different epochs are higher than those measured from the element abundances, and they varies in the range  $0.5Z_{\odot} \leq Z \leq 1Z_{\odot}$  for UGC7576 and  $0.05Z_{\odot} \leq Z \leq 0.45Z_{\odot}$  for UGC9796; 3) for UGC7576, the metallicity remains almost constant along the polar structure.

In the following, we will address how these results reconcile with the theoretical predictions for the cold accretion process and discuss how the SFR and metallicity derived in this work, together with the other two key parameters, i.e. the baryonic mass and kinematics, available by previous studies on these objects, may help to discriminate among the three formation scenarios, in non ambiguous way as done for NGC4650A. All these quantities, for both the PRGs studied in this work and for NGC4650A, are summarized in Tab. 4.

The cold accretion mechanism for disk formation predicts rather low metallicity ( $Z = 0.1Z_{\odot}$ ) (Dekel & Birnboim 2006, Ocvirk et al. 2008, Agertz et al. 2009): such value refers to the time just after the accretion of a misaligned material, so it can be considered as initial value for  $Z$  before the subsequent enrichment. How this may reconcile with the observed metallicity for UGC7576 and UGC9796?

We estimated that the present SFR for the polar structure is  $SFR = 1.9 \times 10^{-5} M_{\odot} \text{yr}^{-1}$  for UGC7576 and  $SFR = 4.2 \times 10^{-6} M_{\odot} \text{yr}^{-1}$  for UGC9796: these values are able to increase the metallicity of about  $0.15Z_{\odot}$  for UGC7576 and  $0.05Z_{\odot}$  for UGC9796 after 1Gyr (see Sec.4): taking into account that the polar structure is very young, less than 1Gyr (Reshetnikov et al., 1994), an initial value of  $Z = 0.1Z_{\odot}$ , at the time of polar structure formation, could be consistent with the today's observed metallicity. Therefore, the cold accretion of gas can be a possible formation scenario for both the PRGs UGC7576 and UGC9796. In the case of UGC7576, one more hint for the cold accretion scenario comes from the fact that the metallicity expected by the present SFR turns to be higher than those directly measured by the chemical abundances: as already suggested for NGC4650A (Spavone et al., 2010), a possible explanation for this observed feature could be the infall of pristine gas (Finlator et al. 2007; Ellison et al. 2008).

Moreover, in the case of UGC7576, the lack of abundance gradient along the polar structure is consistent with the prediction of recent numerical simulations by Rupke et al. (2010) and Kewley & Ellison (2008); they observe flatter metallicity gradients than those observed in typical spiral galaxies, due to the radial inflow of low metallicity gas from outside. For UGC9796, instead, the metallicity derived by the chemical abundances falls near the lower limit of the expected metallicity range; for this reason we cannot definitely rule out other possible formation scenarios.

The high baryonic (gas+stars) masses, the large extensions of the polar structure and the low metallicity observed in these PRGs are not accounted for in the formation of polar rings through the disruption of a dwarf galaxy, which are characterized by higher metallicities ( $1/9Z_{\odot} \div 1/3Z_{\odot}$ ) and lower HI masses ( $\sim 10^7 M_{\odot}$ ; Galametz et al. 2009 and Bekki 2008).

Differently, the tidal accretion scenario, in which gas is stripped from a gas-rich donor in a particular orbital configuration (Bournaud & Combes, 2003), is able to produce wide polar rings and/or disks both around a disk or an elliptical galaxy. In order to consider the accretion hypothesis, we studied the field around these galaxies to see if there are any objects as possible donor galaxy candidates: inside a radius of about 5 times the diameter of both PRGs, as suggested by Brocca et al. (1997), we find that UGC7576 has no close companions, while UGC9796, that is in a small group, has 5 companions (Cox et al., 2006). Therefore, while also the tidal accretion scenario is ruled out for UGC7576, it needs to be envisioned in the case of UGC9796. The VLA images show that UGC9796 and the close companion galaxy MCG+07-31-049 (labelled as 1 in Fig. 8) could be in the orbital configuration needed to form a polar structure through an accretion event (Bournaud & Combes, 2003): in fact, the HI gas in UGC9796, which is all associated with the polar structure, has the outer contours warped away from the poles and, in the SE regions, it extends towards MCG+07-31-049, which has HI distribution extending in a direction perpendicular to that of UGC9796.

In the tidal accretion process, the accreted gas comes only from the outer and more metal-poor regions of the donor galaxy. All the companion galaxies of UGC9796 have an amount of HI gas ( $\sim 10^9 M_{\odot}$ ) comparable with those of this PRG (Cox et al., 2006), but, according to Bresolin et al. (2009), the metallicity of the outer regions of bright spiral galaxies is  $0.2Z_{\odot} \leq Z \leq 1.1Z_{\odot}$  and the observed value for UGC9796,  $Z = 0.100 \pm 0.001Z_{\odot}$ , is below the lower limit.

Given all the evidences shown above, we can give the following conclusions for this work.

The cold accretion of gas by cosmic web filaments could well account for both the low metallicity, the lack of gradient and the high HI content in UGC7576. Moreover, the general underdensity of the environment where this galaxy is, can be consistent with the cold flow accretion of gas as the possible formation mechanism for this object.

For UGC9796 instead, the scenario is slightly more complex. In fact, the low metallicity estimated, even lower than those observed in the outskirts of spiral galaxies is consistent with the formation of disks through cold accretion mechanisms (Dekel & Birnboim 2006, Ocvirk et al. 2008 and Agertz et al. 2009). On the other hand, the tidal accretion scenario cannot be ruled out, given that the galaxy MCG +07-31-049, with its high amount of HI and its orbital configuration, could be a good candidate donor for UGC9796.

*Acknowledgements.* The authors wish to thank the anonymous referee for the detailed and constructive report, and Frederic Bournaud, for many useful discussions and suggestions. M. S. and E. I. wish to thank Massimo Capaccioli for his useful suggestions, which allowed to improve this paper. This work is based on observations made with Telescopio Nazionale Galileo (TNG) under programme ID A21TAC-54.

## References

- Agertz, O., Teyssier, R., & Moore, B. 2009, MNRAS, 397, L64  
 Arnaboldi, M., Oosterloo, T., Combes, F., Freeman, K. C., & Koribalski, B. 1997, AJ, 113, 585

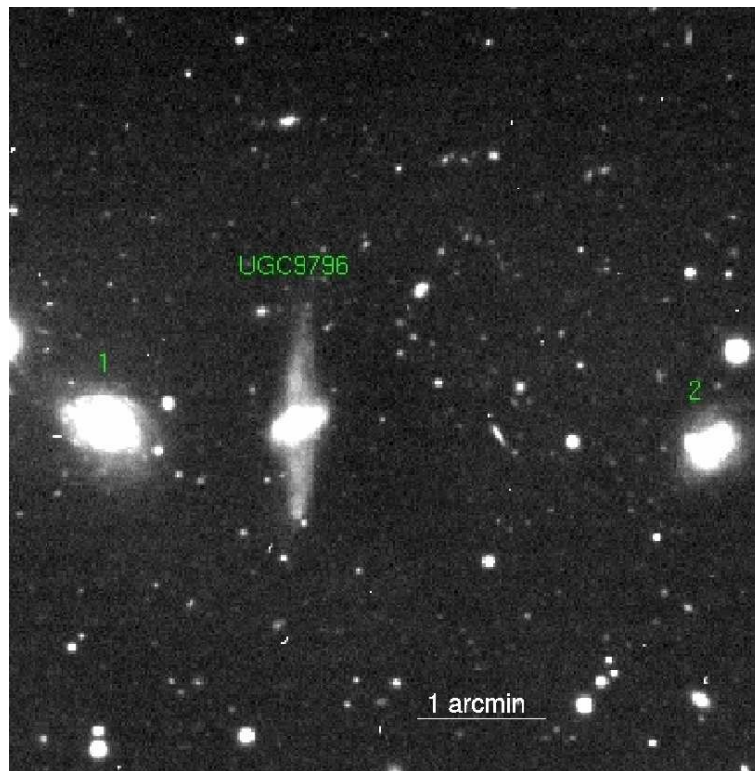


**Fig. 8.** Optical image of UGC9796 and its two nearest companion galaxies, MCG +07-31-049 (number 1) and CGPG 1514.2+4320 (number 2).

- Asplund, M., Grevesse, N., Sauval, A. J., Allende Prieto, C., & Kiselman, D. 2004, *A&A*, 417, 751
- Bekki, K. 1997, *ApJL*, 490, L37
- Bekki, K. 1998, *ApJ*, 499, 635
- Bekki, K. 2008, *ApJL*, 680, L29
- Boissier, S., & Prantzos, N. 1999, *MNRAS*, 307, 857
- Bournaud, F., & Combes, F. 2003, *A&A*, 401, 817
- Bournaud, F., Jog, C. J., & Combes, F. 2005, *A&A*, 437, 69
- Bournaud, F., Jog, C. J., & Combes, F. 2007, *A&A*, 476, 1179
- Bournaud, F., & Elmegreen, B. G. 2009, *ApJL*, 694, L158
- Bresolin, F., Ryan-Weber, E., Kennicutt, R. C., & Goddard, Q. 2009, *ApJ*, 695, 580
- Brocca, C., Bettoni, D., & Galletta, G. 1997, *A&A*, 326, 907
- Brook, C. B., Governato, F., Quinn, T., Wadsley, J., Brooks, A. M., Willman, B., Stulp, A., & Jonsson, P. 2008, *ApJ*, 689, 678
- Brooks, A. M., Governato, F., Quinn, T., Brook, C. B., & Wadsley, J. 2009, *ApJ*, 694, 396
- Brosch, N., Kniazev, A. Y., Moiseev, A., & Pustilnik, S. A. 2009, *arXiv:0910.0589*
- Bruzual, G., & Charlot, S. 2003, *MNRAS*, 344, 1000
- Cardelli, J. A., Clayton, G. C., & Mathis, J. S. 1989, *ApJ*, 345, 245
- Cole, S., Lacey, C. G., Baugh, C. M., & Frenk, C. S. 2000, *MNRAS*, 319, 168
- Conselice, C. J., Bershad, M. A., Dickinson, M., & Papovich, C. 2003, *AJ*, 126, 1183
- Cox, A. L., Sparke, L. S., & van Moorsel, G. 2006, *AJ*, 131, 828
- de Blok, W. J. G., & van der Hulst, J. M. 1998 *A&A*, 335, 421
- De Lucia, G., Springel, V., White, S. D. M., Croton, D., & Kauffmann, G. 2006, *MNRAS*, 366, 499
- Dekel, A., & Birnboim, Y. 2006, *MNRAS*, 368, 2
- Dekel, A., & Birnboim, Y. 2008, *MNRAS*, 383, 119
- Dekel, A., Sari, R., & Ceverino, D. 2009, *ApJ*, 703, 785
- Dekel, A., et al. 2009, *Nature*, 457, 451
- Díaz, A. I., & Pérez-Montero, E. 2000, *MNRAS*, 312, 130
- Ellison, S. L., Patton, D. R., Simard, L., & McConnell, A. W. 2008, *ApJL*, 672, L107
- Elmegreen, D. M., Elmegreen, B. G., Ravindranath, S., & Coe, D. A. 2007, *ApJ*, 658, 763
- Finlator, K., Davé, R., & Oppenheimer, B. D. 2007, *MNRAS*, 376, 1861
- Galametz, M., et al. 2009, *A&A*, 508, 645
- Gallagher, J. S., Sparke, L. S., Matthews, L. D., Frattare, L. M., English, J., Kinney, A. L., Iodice, E., & Arnaboldi, M. 2002, *ApJ*, 568, 199
- Genel, S., et al. 2008, *ApJ*, 688, 789
- Hancock, M., Smith, B. J., Struck, C., Giroux, M. L., & Hurlock, S. 2009, *AJ*, 137, 4643
- Iodice, E., Arnaboldi, M., De Lucia, G., Gallagher, J. S., III, Sparke, L. S., & Freeman, K. C. 2002, *AJ*, 123, 195
- Iodice, E., Arnaboldi, M., Sparke, L. S., Gallagher, J. S., & Freeman, K. C. 2002, *A&A*, 391, 103
- Iodice, E., et al. 2006, *ApJ*, 643, 200
- Katz, N., & White, S. D. M. 1993, *ApJ*, 412, 455
- Katz, N., Quinn, T., Bertschinger, E., & Gelb, J. M. 1994, *MNRAS*, 270, L71
- Kennicutt, R. C., Jr., Roettiger, K. A., Keel, W. C., van der Hulst, J. M., & Hummel, E. 1987, *AJ*, 93, 1011
- Kennicutt, R. C., Jr. 1998, *ARA&A*, 36, 189
- Kereš, D., Katz, N., Weinberg, D. H., & Davé, R. 2005, *MNRAS*, 363, 2
- Keres, D. 2008, 37th COSPAR Scientific Assembly, 37, 1496
- Kewley, L. J., & Ellison, S. L. 2008, *ApJ*, 681, 1183
- Kobulnicky, H. A., & Zaritsky, D. 1999, *ApJ*, 511, 118
- Macciò, A. V., Moore, B., & Stadel, J. 2006, *ApJL*, 636, L25
- Masana, E., Jordi, C., Maitzen, H. M., & Torra, J. 1998, *A&A*, 128, 265
- Matteucci, F., & Francois, P. 1989, *MNRAS* 239, 885
- Naab, T., Johansson, P. H., Ostriker, J. P., & Efstathiou, G. 2007, *ApJ*, 658, 710
- Ocvirk, P., Pichon, C., & Teyssier, R. 2008, *MNRAS*, 390, 1326
- Pagel, B. E. J., Edmunds, M. G., Blackwell, D. E., Chun, M. S., & Smith, G. 1979, *MNRAS*, 189, 95
- Pérez-Montero, E., & Díaz, A. I. 2003, *MNRAS*, 346, 105
- Perez-Montero, E., Garcia-Benito, R., Diaz, A. I., Perez, E., & Kehrig, C. 2009, *arXiv:0901.2274*
- Pilyugin, L. S. 2001, *A&A*, 369, 594
- Pilyugin, L. S., Thuan, T. X., & Vilchez, J. M. 2006, *MNRAS*, 367, 1139
- Radtke, I. R., Eskridge, P. B., & Pogge, R. W. 2003, *Bulletin of the American Astronomical Society*, 35, 757
- Reshetnikov, V. P., Hagen-Thorn, V. A., & Yakovleva, V. A. 1994, *A&A*, 290, 693
- Reshetnikov, V. P., & Combes, F. 1994, *A&A*, 291, 57
- Reshetnikov, V., & Sotnikova, N. 1997, *A&A*, 325, 933
- Robertson, B. E., & Bullock, J. S. 2008, *ApJL*, 685, L27
- Roškar, R., Debattista, V. P., Brooks, A. M., Quinn, T. R., Brook, C. B., Governato, F., Dalcanton, J. J., & Wadsley, J. 2010, *MNRAS*, 408, 783

- Rupke, D. S. N., Kewley, L. J., & Barnes, J. E. 2010, *ApJL*, 710, L156  
Schechter, P. L., Sancisi, R., van Woerden, H., & Lynds, C. R. 1984, *MNRAS*, 208, 111  
Spavone, M., Iodice, E., Arnaboldi, M., Gerhard, O., Saglia, R., & Longo, G. 2010, *ApJ*, 714, 1081  
Springel, V., & Hernquist, L. 2005, *ApJL*, 622, L9  
Swaters, R. A., & Rubin, V. C. 2003, *ApJL*, 587, L23  
Tremonti, C. A., et al. 2004, *ApJ*, 613, 898  
Whitmore, B. C., Lucas, R. A., McElroy, D. B., Steiman-Cameron, T. Y., Sackett, P. D., & Olling, R. P. 1990, *AJ*, 100, 1489

**Table 1.** Global properties of UGC7576 and UGC9796 compared to those observed for NGC4650A.

Parameter	UGC7576	UGC9796	NGC4650A
R.A. (J2000)	12h27m41.8s	15h15m56.3s	12h44m49.0s
Decl. (J2000)	+28d41m53s	+43d10m00s	-40d42m52s
Helio. radial velocity	7022 km/s	5406 km/s	2880 km/s
Redshift	0.02342	0.01832	0.009607
Distance	94 Mpc	72 Mpc	38 Mpc
<i>Central galaxy</i>			
$M_B$	-19.15	-17.93	-18.83
B-V	+0.84	+0.92	+0.78
V-R	+0.46	+0.55	
<i>Polar structure</i>			
$M_B$	-17.5	-17.0	-17.0
$M(HI)(M_\odot)$	$2.7 \times 10^9$	$2.6 \times 10^9$	$8.0 \times 10^9$ <sup>a</sup>
$M(HI)/L_B$	0.6	1.5	4
B-V	+0.70 <sup>b</sup>	+0.57 <sup>b</sup>	+0.26 <sup>c</sup>
$\mu_B$	24.3	24.5	22.6
$R_{25}$	13.6	10.8	7.0
$r_{max}$	40''	60''	40''

**Notes.** <sup>(a)</sup> Arnaboldi et al. 1997 <sup>(b)</sup> Reshetnikov et al. 1994 <sup>(c)</sup> Iodice et al. 2002

**Table 2.** Observed and De-Reddened emission line fluxes relative to  $H_\beta$ .

line	$\lambda$ (Å)	Observed flux relative to $H_\beta$	De-Reddened flux relative to $H_\beta$
UGC9796			
[OII]	3727	8.9	6.8
[OIII]	4959	5.0	5.1
[OIII]	5007	8.7	9.0
$H_\gamma$	4340	0.9	0.8
$H_\alpha$	6563	2.2	2.8
UGC7576			
[OII]	3727	2.5	2.8
[OIII]	4959	1.5	1.51
[OIII]	5007	1.7	1.71
$H_\gamma$	4340	1.1	1.15
$H_\alpha$	6563	3.2	2.9

**Table 3.** Oxygen abundances and metallicities of UGC7576 and UGC9796.

Parameter	UGC7576	UGC9796
$12 + \log(O/H)^a$	$8.5 \pm 0.5$	$7.7 \pm 1$
$Z/Z_\odot^a$	$0.4 \pm 0.002$	$0.1 \pm 0.001$

**Notes.** <sup>(a)</sup> Spavone et al. (2010) derived the following values of oxygen abundance and metallicity for NGC4650A:  $12 + \log(O/H) = 8.2 \pm 0.2$  and  $Z/Z_\odot = 0.2 \pm 0.002$

**Table 4.** Discriminant parameters between different formation scenarios

PRG	$M_b^{HG}$ ( $M_\odot$ )	$M_b^{PD}$ ( $M_\odot$ )	$V_{eq}$ (km/s)	$V_{eq}/V_{PD}$	$\sigma_0$ (km/s)	$M_b^{HG}/M_b^{PD}$	$v/\sigma$	$Z_{est}$ ( $Z_\odot$ )	$Z_{exp}$ ( $Z_\odot$ )
UGC7576	$7.86 \times 10^9$	$2.88 \times 10^9$	212	0.96	116	2.73	1.8	$(0.400 \pm 0.002)$	$(0.5 \div 1)$
UGC9796	$1.0 \times 10^{10}$	$3.05 \times 10^9$	157	1.08	73	3.28	2.15	$(0.100 \pm 0.001)$	$(0.05 \div 0.45)$
NGC4650A	$5 \times 10^9$	$12 \times 10^9$	90	0.75	70	0.42	1.28	$(0.200 \pm 0.002)$	$(1.02 \div 1.4)$